Long-Wavelength Infrared Digital Focal Plane Arrays for Earth Remote Sensing Applications

Sarath Gunapala, Sir Rafol, David Ting, Alexander Soibel, Arezou Khoshakhlagh, Sam Keo, Brian Pepper, Anita Fisher, Edward Luong, and Cory Hill

Center for Infrared Photodetectors, Jet Propulsion Laboratory, California Institute of Technology
Pasadena, California, USA

Arvind D'Souza and Christopher Masterjohn

DRS Network & Imaging Systems, Inc.
Cypress, California, USA

Sachidananda Babu and Parminder Ghuman

NASA Earth Science Technology Office
Greenbelt, Maryland, USA

***Index terms*— type-II superlattice, infrared detector, quantum efficiency, digital, focal plane array**

I. Introduction

In this presentation, we will report our recent efforts in achieving high performance in Antimonides type-II strained-layer superlattice (T2SLS) based infrared photodetectors using the barrier infrared detector (BIRD) device architecture. The recent emergence of barrier infrared detectors such as the nBn [1] and the XBn [2] have resulted in mid-wave infrared (MWIR) and long-wave infrared (LWIR) detectors with substantially higher operating temperatures than previously available in III-V semiconductor based MWIR and LWIR detectors. The initial nBn devices used either InAs absorber grown on InAs substrate, or lattice-matched InAsSb alloy grown on GaSb substrate, with cutoff wavelengths of ~3.2 μm and ~4 μm, respectively. While these detectors could operate at much higher temperatures than existing MWIR detectors based on InSb, their spectral responses do not cover the full (3 – 5.5 μm) MWIR atmospheric transmission window. There also have been nBn detectors based on the InAs/GaSb type-II superlattice absorber [3].

II. Barrier Infrared Detectors

Much has been discussed in the literature about the nBn and related devices, including XBn barrier photodetector [4-5], and unipolar barrier photodiode [5], since the publication of the influential paper entitled "nBn detector, an infrared detector with reduced dark current and higher operating temperature" by Maimon and Wicks in 2006 [1]. Common to this family of devices is the unipolar barrier. The term "unipolar barrier" was used recently to describe a barrier that can block one carrier type (electron or hole) but allows the un-impeded flow of the other [1, 4-5]. The concept of the unipolar barrier has been around long before they are called as such. The double-heterostructure (DH) laser, which makes use of a pair of complementary unipolar barriers, was first described in 1963 [6], soon after the birth of the concept of heterostructure devices.

The ideal nBn structure would have two n-type region (n) separated by a larger bandgap, undoped barrier layer (B), where the n-B heterojunctions have a larger conduction band offsets and zero valence band offsets. Such a barrier would block majority carrier electrons, but pass photogenerated holes. The nBn infrared detector is designed to reduce dark current (noise) without impeding photocurrent (signal). Central to the nBn operation is the strong suppression of generation-recombination (G-R) dark current due to Shockley-Read-Hall (SRH) processes. The nBn infrared detector is designed to reducing dark current (noise) without impeding photocurrent (signal).

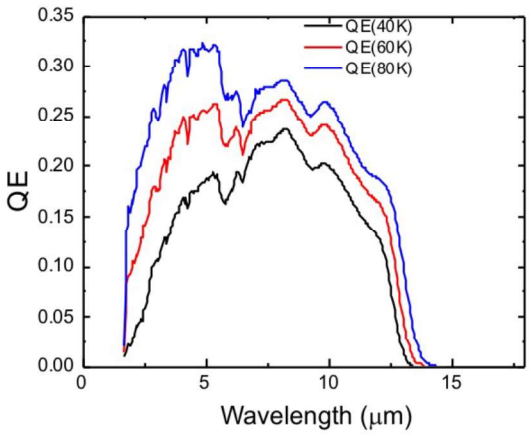

Figure 1. Backside illuminated spectral quantum efficiency (QE) for an LWIR detector measured at temperatures ranging from 40K to 80K.

Another important aspect of nBn and related structures is their effectiveness in reducing surface leakage current. The top surface of the active narrow gap absorber in the nBn detector is covered by the wide band gap barrier layer, and therefore does not need additional passivation to suppress surface leakage [1]. In a focal plane array (FPA) configuration, the array of top contacts could be defined by etching through the top contact layer but not the barrier layer [1]. In this

configuration, the narrow gap absorber is not exposed, and therefore does not contribute to surface leakage. Finally, even in a deep-etched mesa configuration, where the side walls of the narrow gap absorber are fully exposed, the barrier can still block electron surface leakage effectively [1, 5]. An important aspect of the nBn detector (and unipolar barrier detector architecture in general) is the ability to block majority carriers without impeding the flow of minority carriers.

The InAs/InAsSb (Gallium-free) T2SLS has emerged as an alternative adjustable bandgap, broad-band III-V IR detector material to the more established InAs/GaSb type-II superlattice (T2SL). Recently, there has been growing interest in this material as an infrared detector absorber due to longer MWIR and LWIR minority carrier lifetimes in InAs/InAsSb strained-layer superlattice (SLS) than in InAs/GaSb superlattice (SL) and demonstrated an InAs/InAsSb SLS LWIR photodetector based on the nBn device design [7]. The T2SLS material can be grown on InAs or GaSb substrates, GaSb is available in 2", 3", 4" and 6" diameters formats.

III. LWIR BIRD Focal Plane Array

An InAs/InAsSb SLS nBn structure was grown on a 4-inch diameter low Te-doped GaSb (100) substrate in a Veeco Applied-Epi Gen III molecular beam epitaxy chamber equipped with valved cracking sources for the group V Sb2 and As2 fluxes. The nBn architecture is used for G-R and surface-leakage dark current suppression. Square mesa photodiodes of area 250µm x 250µm were fabricated along with detector arrays for responsivity and dark current measurements. The devices were not passivated nor treated with anti-reflection coating. Figure 1 shows the spectral quantum efficiency (QE) derived from back-side illuminated (through the GaSb substrate) spectral responsivity measured at temperatures ranging from 40K to 80K; the QE has not been corrected for substrate reflection or transmission. Accordingly, the spectral QE for 40K and 80K was taken at -50mV. The cutoff, taken at the wavelength at which the QE is 50% of that at λ=12.5µm.

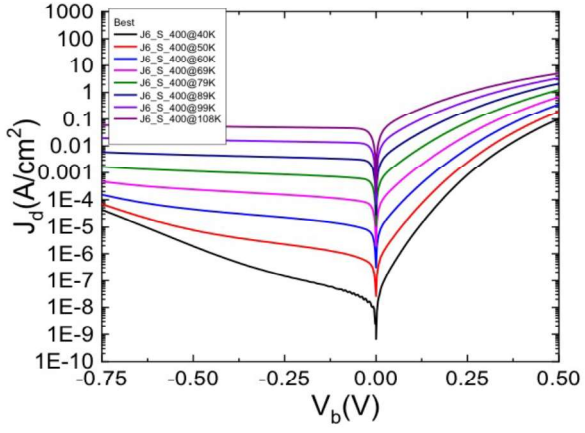

Figure 2. Dark current density (J_d) as a function of applied bias, measured at temperatures ranging from 40K to 108K.

Figure 2 shows the measured dark current density as a function of applied bias for temperatures ranging from 40K to 108K. The -50mV dark current density at 60K is 2.6×10^{-5} A/cm^2. The presence of G-R dark current is apparent from the shapes of the J-V curves in Fig. 2 at temperatures below 60K; tunneling current can also be seen at lower temperatures and high reverse bias.

The detector material was used to fabricate 24µm pitch, 640x512 format arrays and hybridized to the SBF-193 readout integrated circuit (ROIC). The detector mesas are etched to just below the barrier; the pixels are not fully reticulated.

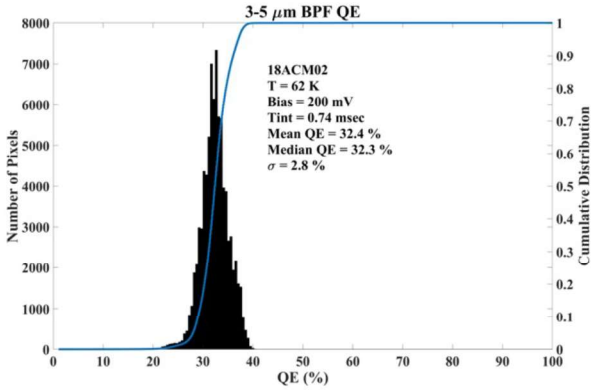

Figure 3. 3-5µm broad-bandpass filter QE of the LWIR BIRD focal plane array (FPA) at 62K.

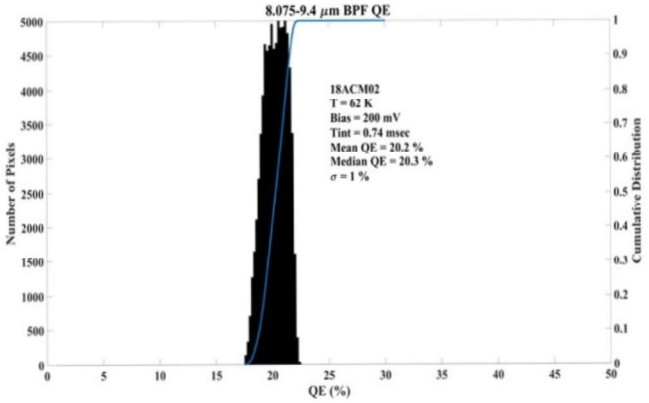

Figure 4. 8-9.4µm broad-bandpass filter QE of the LWIR BIRD focal plane array (FPA) at 62K.

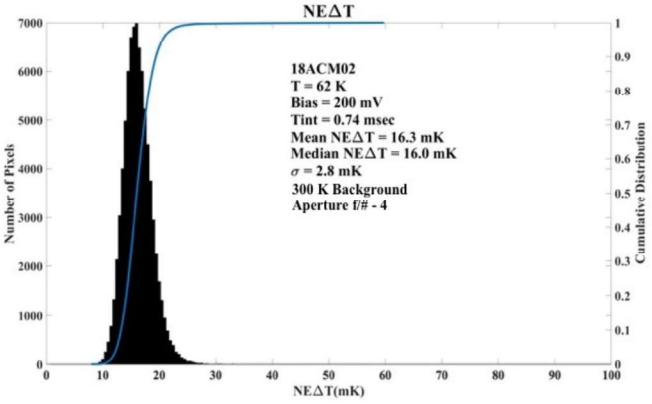

Figure 5. Noise equivalent temperature difference (NEDT) of the 12.5µm cutoff BIRD FPA at 62K.

The noise equivalent temperature difference (NEΔT) provides the thermal sensitivity of an infrared imaging system and it is a very useful diagnostic tool to evaluate the full operational performance available. It is defined as the minimum temperature difference required at the target to produce unity signal-to-noise-ratio. Sequence of consecutive frames is collected for equivalent noise determination as well as other optical properties of FPA. The photo response matrices of FPA is derived at the low and high blackbody temperatures (i.e., 295 K and 305 K), and temporal noise matrix of FPA is estimated at the mid-point temperature by taking 64 frames of data. The temporal NEΔT of pixels are numerically evaluated from the relations, $NE\Delta T = \sigma_{Temporal}\Delta T/[Mean(T_H) - Mean(T_L)]$. The mean signal $Mean(T_L)$ and $Mean(T_H)$ are evaluated at blackbody temperatures of T_L = 295 K and T_H = 305 K. The temporal noise is measured at 300K using 64 frames, and ΔT ~10 K.

The experimentally measured NEΔT histograms distributions of 640x512 pixels LWIR BIRD FPA at 62K operating temperature with blackbody temperature of 300 K and f/4 cold stop is shown in the Fig. 5. The experimentally measured NEΔT of 16.3mK is in fair agreement with the estimated NEΔT value based on the results of a single element test detector data.

Figure 6. An image taken with the 640x215 pixels LWIR Ga-free T2SLS FPA. Array operated at 62K with NEΔT of 16.3mK with f/4 optics at 300K background.

IV. Digital Read Out Integrated Circuit

Infrared FPAs generally use non-silicon detector arrays to convert the infrared signal into an electrical signal. These detector arrays are hybridized via indium bump bonding process to a read out integrated circuit (ROIC). Conventional ROICs are based on analog electronic circuits. The modern ROICs are digital ROICs (DROICs). Conventional analog ROICs store charges at individual ROIC pixels and route them out via output taps to off-chip analog-to-digital converters (ADCs) or route them to on-chip column parallel ADCs. This method requires a very large ROIC in-pixel well depth to achieve high signal-to-noise-ratio (SNR). In DROICs the charges get digitized at ROIC individual pixel level with a counter by incrementing each time a small charge bucket gets filled. Ideally, this could provide a very high effective well depth for DROIC pixels compared to conventional analog ROIC pixels. Total well depth of DROIC pixel is given by the size of the charge bucket times the number of counts of the in-pixel counter [8-9].

The ultimate sensitivity (i.e., highest SNR) of an infrared FPA is determined by the maximum well depth of the ROIC pixels assuming the total noise of the FPA is determined by the shot noise (i.e., statistical fluctuations of the signal) of the photocurrent. Therefore, to achieve the maximum SNR,

$$SNR_{Max} = \frac{Signal_{Max}}{Noise} = \sqrt{Well\ Depth_{Max}}$$

Where, $Signal_{Max}$ is the maximum signal and noise is Poisson process limited statistical variation associated with the photocurrent. Thus, a maximum well depth of 25 million electrons yields SNR of 5,000 and well depth of 100 million electrons yields SNR of 10,000. Therefore, a DROIC with higher bit counter could provide a higher SNR or could operate a DFPA at higher operating temperature with same SNR as a conventional FPA (i.e., same detector array with an analog ROIC).

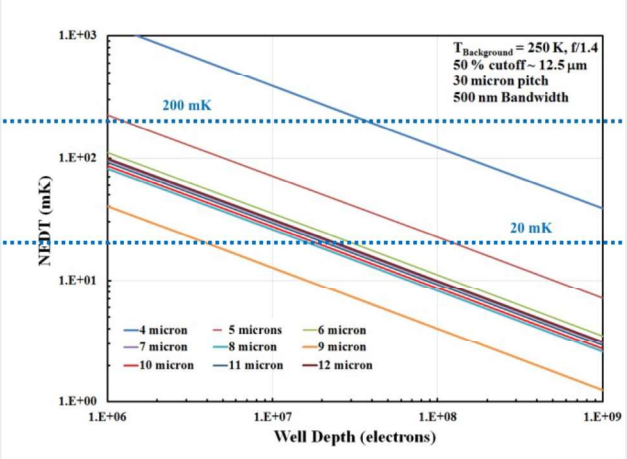

Figure 7. NEΔT vs. ROIC well depth as a function of wavelength (from 4-12µm) for the 12.5µm cutoff LWIR BIRD FPA operating at 65K with 250K background and f/1.4 aperture. Dotted horizontal lines represent the 20mK and 200mK NEΔT.

Figure 7 shows a case study performed with the experimental values obtained from the 12.5µm cutoff LWIR BIRD FPA operating at 65K with 250K background and f/1.4 aperture. We assumed 0.5µm bandpass for each wavelength (i.e., similar to TIRS instrument on Landsat 8). Figure 7 clearly shows that LWIR BIRD FPA operating at 65K can easily achieve 20mK NEΔT with a DROIC with well capacity of 25 million electrons for all wavelengths from 6-12µm. As shown in Fig. 7, same FPA could also achieve 20mK NEΔT performance from 5-12µm if DROIC could provide 100 million electrons well depth. These kind of well depths (or even higher) are nominal to all DROICs.

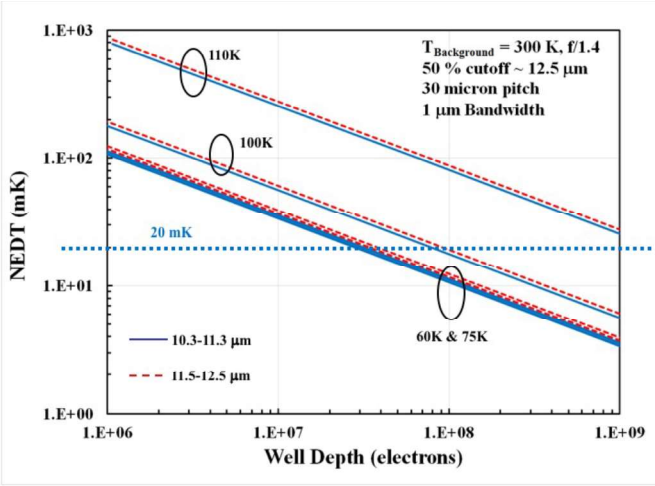

Figure 8. NEΔT vs. ROIC well depth as a function of LWIR BIRD FPA operating temperature for two Landsat wavelength bands (from 10.3-11.3µm and 11.5-12.5µm) with 250K background and f/1.4 aperture.

Figure 8 shows a case study performed with the experimental values obtained from the 12.5µm cutoff LWIR BIRD FPA operating at various temperatures from 60K to 110K with 250K background and f/1.4 aperture. Fig. 8 clearly shows the two LWIR Landsat bands, from 10.3-11.3µm and 11.5-12.5µm can achieve 20mK NEΔT with a DROIC with 100 million electrons well depth. Furthermore, LWIR BIRD FPAs could operate at even higher temperature with DRIOCs having greater effective well depths.

V. Summary

Ga-free T2SLS LWIR BIRD FPA could easily operates at 20K higher operating temperature (HOT) (i.e. compared to QWIP FPA) due to the strong suppression of G-R dark current due to SRH processes as explained earlier. The light trapping resonator pixel concept offers a very effective solution to increase the QE of LWIR T2SL BIRDs. Another 20K higher operating temperature advantage can be achieved when we further improve the performance by hybridizing the T2SLS LWIR BIRD detector array to the high-dynamic range DROIC from DRS. Therefore, a T2SLS LWIR BIRD DFPA can easily operates at much higher operating temperature compared to a conventional LWIR FPA.

Acknowledgement

The authors thank the NASA Earth Science Technology Office and Jason Hyon and Eastwood Im of Jet Propulsion Laboratory for encouragement and support. The research described in this paper was carried out at the Jet Propulsion Laboratory, California Institute of Technology, under a contract with the National Aeronautics and Space Administration.

References

1. S. Maimon and G. W. Wicks, "nBn detector, an infrared detector with reduced dark current and higher operating temperature", Appl. Phys. Lett. 89, 151109 (2006).

2. P. C. Klipstein, "XBn barrier photodetectors for high sensitivity and high operating temperature infrared sensors," Proc. SPIE 6940, 6940–2U (2008).

3. J. F. Klem, S.R. Kurtz, A. Datye, "Growth and properties of GaAsSb/InGaAs superlattices on InP", J. Crystal Growth 111(1-4), 628-632 (1991).

4. David Z Ting, Alexander Soibel, Arezou Khoshakhagh, Linda Höglund, Sam A Keo, Sir B. Rafol, Cory J Hill, Anita M Fisher, Edward M Luong, Jean Nguyen, John K Liu, Jason M Mumolo, Brian J Pepper, Sarath D Gunapala, "Antimonide type-II superlattice barrier infrared detectors", SPIE Defense+ Security, 101770N-101770N-10, (2017).

5. D. Z. Ting, A. Soibel, A. Khoshakhlagh, S. B. Rafol, S. A. Keo, L. Höglund, A. M. Fisher, E. M. Luong, and S. D. Gunapala, "Mid-wavelength high operating temperature barrier infrared detector and focal plane array", Appl. Phys. Lett. 113 , 021101 (2018). doi: 10.1063/1.5033338

6. H. Kroemer, "A proposed class of heterojunction injection lasers," Proc. IEEE 51(12), 1782 (1963).

7. E. H. Steenbergen, B. C. Connelly, G. D. Metcalfe, H. Shen, M. Wraback, D. Lubyshev, Y. Qiu, J. M. Fastenau, A. W. K. Liu, S. Elhamri, O. O. Cellek, and Y.-H. Zhang, "Significantly improved minority carrier lifetime observed in a long-wavelength infrared III-V type-II superlattice comprised of InAs/InAsSb", Appl. Phys. Lett. 99, 251110 (2011).

8. Kenneth I. Schultz, Michael W. Kelly, Justin J. Baker, Megan H. Blackwell, Matthew G. Brown, Curtis B. Colonero, Christopher L. David, Brian M. Tyrrell, and James R. Wey, "Digital-Pixel Focal Plane Array Technology", LINCOLN LABORATORY JOURNAL, Vol. 20 (2), 36-51 (2014).

9. M. W. Kelly, R. Berger, *et al*., "Design and Testing of an All-Digital Readout Integrated Circuit for Infrared Focal Plane Arrays," Proc. SPIE, 5902, (2005).